

## Seismic analysis of rectangular alluvial valleys subjected to incident SV waves by using the spectral finite element method

J. Najafizadeh<sup>1</sup>, M. Kamalian<sup>1\*</sup>, M.K. Jafari<sup>1</sup>, N. Khaji<sup>2</sup>

Received: May 2013, Revised: April 2014, Accepted: June 2014

### Abstract

*In this paper, an advanced formulation of the spectral finite element method (SFEM) is presented and applied in order to carry out site response analysis of 2D topographic structures subjected to vertically propagating incident in-plane waves in time-domain. The accuracy, efficiency and applicability of the formulation are demonstrated by solving some wave scattering examples. A numerical parametric study has been carried out to study the seismic response of rectangular alluvial valleys subjected to vertically propagating incident SV waves. It is shown that the amplification pattern of the valley and its frequency characteristics depend strongly on its shape ratio. The natural frequency of the rectangular alluvial valley decreases as the shape ratio of the valley decreases. The maximum amplification ratio along the ground surface occurs at the center of the valley. A simple formula has been proposed for making initial estimation of the natural period of the valley in site effect microzonation studies.*

**Keywords:** Spectral finite element, Amplification, Time-domain, Topography effects, Wave propagation.

### 1. Introduction

Nowadays, it is well founded that 2D topographical effects influence highly seismic response of the ground surface and the distribution of damages due to the earthquake. 2D topographical effects may be considerable when the topography dimensions (hill and valley) are comparable with seismic wavelengths [1]. The frequency range of a strong earthquake is from 0.3 to 10 Hz, and the speed range of the seismic waves of alluvial layers varies from 0.1 to 3 km/s. Therefore, the seismic behavior of topographical structures may be considerably influenced by their multidimensional geometry.

In addition to the importance of 2D topographical effects on seismic behavior, careful and efficient solution with less computational efforts has been a matter of concern to the researchers in this field. So, it made the researchers use suitable numerical methods for solution of wave propagation phenomenon or dynamic analysis of 2D topography's effects. Examples of the most efficient numerical methods used by the researchers during the recent decade for seismic analysis of topographic areas are the conventional Finite Element Method (FEM), the Boundary Element Method (BEM), and the Spectral Finite

Element Method (SFEM).

Examples of the most important numerical works done in the field of the FEM, are the works of Zhao and Valliappan [2,3], Sincaian and Oliveira [4] in investigation of seismic response of valleys and hills. Bouchon [1] was the first researcher who investigated the effect of hills on seismic behavior of the ground surface by using the BEM. Later, using this method, Geli et al [5] studied the effect of sub-surface layering and the presence of adjacent irregularities on the seismic response of hills. In 2001-2009, using the BEM or a combination of BEM with the FEM, Kamalian et al [6-16] conducted an extensive parametric study in order to investigate seismic behavior of various hills and valleys. In 2005, studying the Grenoble valley in France and using the SFEM numerical method, Chaljub [17] investigated the seismic behavior of this topographic structure.

The SFEM is a high-order technique with important computational advantageous over the conventional FEM as well as the BEM. A degree of accuracy similar to the conventional FEM is achieved from it by using fewer meshing points. For this reason, it improves drastically the efficiency as well as the accuracy of the computational resources. The SFEM which has all advantages of the classic FEM, including the capability to solve non-linear problems in contrast to the BEM, has been strengthened with a special group of interpolation functions. These interpolation functions enable the SFEM to pass a wider range of wavelengths in the elements with more careful and less computational efforts than that of the conventional FEM [18].

\* Corresponding author: KAMALIAN@iiees.ac.ir

<sup>1</sup> Geotechnical Engineering Research Center, International Institute of Earthquake Engineering and Seismology (IIEES)

<sup>2</sup> Faculty of Civil and Environmental Engineering, Tarbiat Modares University

The SFEM was first used by Patera [19] in 1984 in order to solve some problems in Fluid Mechanics. Later, Cohen et al [20] (1993) applied this method in order to solve some wave propagation problems. In 1997-2000, Komatitsh [21,22,23,24] showed the validity, accuracy, efficiency, and stability of the SFEM in solving many wave propagation problems such as the Lamp problem, Garion problem and etc. In 2002 and 2005, Komatitsh et al [25, 26] modeled the earthquake wave propagation in the earth's domain by using the SFEM. In this research, records of the artificially-produced earthquake were compared to the records of the real earthquakes including Bolivia earthquake in 1994, Columbia earthquake in 1997, and the earthquake of Denali fault in 2002 in Alaska. The results indicated that SFEM was highly accurate in solving the problems of wave propagation. In 1999, Komatitsh et al [27] showed higher degrees of efficiency and accuracy of the SFEM in the wave propagation in the problems with topographical conditions, 3D hills and ditch.

In this research, an advanced formulation of the SFEM is presented and applied in order to carry out site response analysis of 2D rectangular alluvial valleys subjected to vertically propagating incident SV waves in time-domain. The behavior of the alluvial is assumed isotropic linear elastic and the surrounding rock is assumed to behave rigidly. The most important aim of this research was to find initial answers to the following questions: How does the shape ratio (ratio of height to half-width) of an alluvial rectangular valley affect its amplification potential and its frequency characteristics? Can a uniform characteristic frequency be detected for all points along the ground surface? Where does the maximum amplification ratio occur along the ground surface?

Although the nonlinear SFEM code developed in this research is capable of executing seismic response analysis of sites subjected to vertically propagating P waves, too, but the parametric study of this research was restricted to SV waves. The reason is that the material damping of soil or rock due to P waves is usually higher than the material damping due to S waves. So, P waves attenuate much more rapidly than S waves and this makes the S waves

$$\begin{aligned} \int_{\Omega} \sigma_{ij,j} \cdot \delta u_i \cdot d\Omega &= \int_{\Omega} (\sigma_{ij} \cdot \delta u_i)_{,j} \cdot d\Omega - \int_{\Omega} \sigma_{ij} \cdot \delta u_{i,j} \cdot d\Omega = \\ &= \int_{\Gamma} \sigma_{ij} \cdot \delta u_i \cdot n_j \cdot d\Omega - \int_{\Omega} \sigma_{ij} \cdot \delta \varepsilon_{ij} \cdot d\Omega = \int_{\Gamma} t_i \cdot \delta u_i \cdot d\Gamma - \int_{\Omega} \sigma_{ij} \cdot \delta \varepsilon_{ij} \cdot d\Omega \end{aligned} \quad (3)$$

Therefore, Eq. (2) will be written as below:

$$\int_{\Gamma} t_i \cdot \delta u_i \cdot d\Gamma - \int_{\Omega} \sigma_{ij} \cdot \delta \varepsilon_{ij} \cdot d\Omega + \int_{\Omega} F_i \cdot \delta u_i \cdot d\Omega - \int_{\Omega} \rho \cdot \ddot{u}_i \cdot \delta u_i \cdot d\Omega = 0 \quad (4)$$

In the Finite Element Method, the level  $\Omega$  is divided into  $m$  small elements. In each of the elements, we have:

$$\begin{aligned} u^m(x, y) &= N^m(x, y) \cdot U \\ \varepsilon^m(x, y) &= B^m(x, y) \cdot U \\ \sigma^m(x, y) &= C^m \varepsilon^m(x, y) \end{aligned}$$

have greater displacement (or acceleration) amplitudes and more importance compared to the P waves, particularly in far fields. In addition, in case of vertically propagating incident waves, S waves produce horizontal vibration of the ground surface which is usually more destructive to the buildings than the vertical movement produced by P waves.

## 2. Formulation of Spectral Finite Elements of the Problem

### 2.1. Governing Equations

In this section, formulation of the governing equations and their matrix form are presented. In the following, environmental issues is assumed isotropic, homogeneous, small-displacement with linear elastic behavior. The equilibrium equations for an elastic bounded medium  $\Omega \subset R_d$  subjected to an external body-force  $f_i$  is described by (1):

$$\sigma_{ij,j} + f_i = \rho \ddot{u}_i \quad , \quad i = 1, \dots, d \quad (1)$$

where  $\ddot{u}_i = \partial^2 u_i / \partial t^2$  is the second derivative of displacement of the medium with respect to time;  $\rho$ , the mass density, and  $\sigma_{ij}$  denotes the stress tensor components. Then, using the weighted residual approach, weak formulation of the governing equations and their matrix form are extracted.

If we multiply Eq. (1) by the weight function  $\delta u_i$ , and the product integration on the level  $\Omega$  is set equal to zero, this gives (2).

$$\int_{\Omega} (\sigma_{ij,j} - \rho \cdot \ddot{u}_i + F_i) \cdot \delta u_i \cdot d\Omega = 0 \quad (2)$$

The first expression of the above integral can be rewritten by using the integration by parts as below:

where  $U$  is the vector of node displacement. Therefore, Eq. (4) is given as follows:

$$\sum_m \int_{\Gamma_m} t_i^m \cdot \delta u_i^m \cdot d\Gamma_m - \sum_m \int_{\Omega_m} \sigma_{ij}^m \cdot \delta \varepsilon_{ij}^m \cdot d\Omega_m + \sum_m \int_{\Omega_m} F_i^m \cdot \delta u_i^m \cdot d\Omega_m - \sum_m \int_{\Omega_m} \rho \cdot \ddot{u}_i^m \cdot \delta u_i^m \cdot d\Omega_m = 0 \quad (5)$$

The individual expressions of Eq. (5) can be rewritten after discretization in space as following:

$$\begin{aligned} \int_{\Gamma_m} t_i^m \cdot \delta u_i^m \cdot d\Gamma_m &= \delta U^T \cdot \int_{\Gamma_m} N^{mT} \cdot t^m \cdot d\Gamma_m = \delta U^T \cdot f_{\Gamma_m-u} \\ \int_{\Omega_m} \sigma_{ij}^m \cdot \delta \varepsilon_{ij}^m \cdot d\Omega_m &= \delta U^T \cdot \int_{\Omega_m} B^{mT} \cdot C^m \cdot B^m \cdot d\Omega_m \cdot U = \delta U^T \cdot K^m \cdot U \\ \int_{\Omega_m} F_i^m \cdot \delta u_i^m \cdot d\Omega_m &= \delta U^T \cdot \int_{\Omega_m} N^{mT} \cdot F^m \cdot d\Omega_m = \delta U^T \cdot f_{\Omega_m-u} \\ \int_{\Omega_m} \rho \cdot \ddot{u}_i^m \cdot \delta u_i^m \cdot d\Omega_m &= \delta U^T \cdot \int_{\Omega_m} N^{mT} \cdot \rho \cdot N^m \cdot d\Omega_m \cdot \ddot{U} = \delta U^T \cdot M^m \cdot \ddot{U} \end{aligned} \quad (6)$$

Now, if the above definitions are replaced in Eq. (5), after removing the coefficient  $\delta U^T$ , the following matrix form of the governing equation will be obtained:

$$M \cdot \ddot{U} + K \cdot U = F \quad (7)$$

where:

$$\begin{aligned} K &= \sum_m K^m \\ M &= \sum_m M^m \\ F &= \sum_m (f_{\Gamma_m-u} + f_{\Omega_m-u}) \end{aligned} \quad (8)$$

If material damping is assumed in the medium, Eq. (7) can be rewritten as follows:

$$M \cdot \ddot{U} + C \cdot \dot{U} + K \cdot U = F \quad (9)$$

In this research, the well known Rayleigh damping mechanism was used which can be expressed proportional to the mass and stiffness matrixes as follows: [30]

$$C = a_0 M + a_1 K \quad (10)$$

## 2.2. Mesh definition

A spectral element approximation of Eq. (2) and its solution are obtained as follows. First, the domain  $\Omega$  is decomposed into some quadrilateral (2D) non-overlapping elements  $\Omega_e$ . Second, an expansion in terms of a tensor-product of  $N$ th-order orthogonal polynomials is used to approximate solution, data, geometry and physical properties on each element. Each quadrilateral spectral element is analogous to the square. Hence, we adopt a suitable mapping between the square (master/reference element) and each spectral element (Fig. 1). The master element (base square) is defined in terms of  $\eta$ ,  $\xi$  as follows:

$$-1 \leq \xi \leq 1, \quad -1 \leq \eta \leq 1 \quad (11)$$

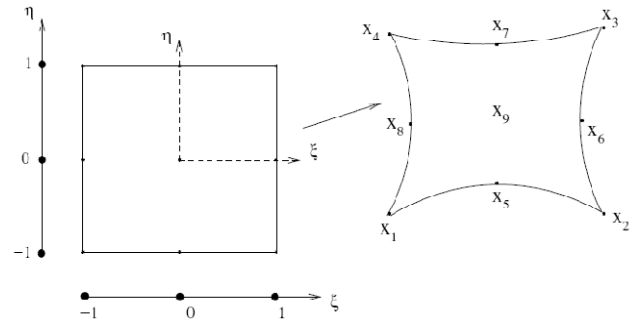


Fig. 1 Mapping a 2D surface element to the master square

which are sometimes referred to as the initial coordinates. In addition, each quadrilateral element  $\Omega_e$  consists of  $n_n$  nodes. The relation between a point  $(x,y)$  within each quadrilateral element is given and a point  $(\xi,\eta)$  in the master element may thus be written in the form:

$$x(\xi,\eta) = \sum_{n=1}^{n_n} N_n(\xi,\eta) x_n \quad (12)$$

$$y(\xi,\eta) = \sum_{n=1}^{n_n} N_n(\xi,\eta) y_n \quad (13)$$

where  $x_n$  and  $y_n$  are the coordinates of  $n$ th node in the quadrilateral element domain  $\Omega_e$ , and  $N_n(\xi,\eta)$  is the  $n$ th node's shape function as :

$$N_n(\xi,\eta) = h_n^{\eta_i}(\xi) h_n^{\xi_i}(\eta) \quad (14)$$

in which  $h_n^{\eta_i}(\xi)$  and  $h_n^{\xi_i}(\eta)$  denote the  $n$ th node's shape functions in  $\eta$  &  $\xi$  natural coordinates directions, respectively. The shape functions  $N_n(\xi,\eta)$  are products of Lagrange polynomials in directions of  $\eta$  &  $\xi$ . Moreover

the Lagrange polynomials used in this research are in the

$$h_n^{n_i}(\xi) = \frac{(\xi - \xi_1)(\xi - \xi_2)\dots(\xi - \xi_{n-1})(\xi - \xi_{n+1})\dots(\xi - \xi_{n_i+1})}{(\xi_n - \xi_1)(\xi_n - \xi_2)\dots(\xi_n - \xi_{n-1})(\xi_n - \xi_{n+1})\dots(\xi_n - \xi_{n_i+1})} \quad (15)$$

$$-1 \leq \xi \leq 1, \quad n = 1, \dots, n_i + 1 \quad (16)$$

Note that as a result of this definition, the Lagrange polynomials return either zero or one at any given control point:

$$h_n(\xi_m) = \delta_{nm} \quad (17)$$

Where  $\delta$  denotes the Kronecher delta.

In the Spectral Finite Element Method, control points  $\xi_p$ ,  $p = 0, \dots, n_i$  needed in defining the equation (15) in Lagrange polynomials of degree  $n_i$  are placed at special positions called Legendre-Gauss-Lobatto (LGL) points. Place of the control points is determined through solving the following equations:

$$(1 - \xi^2) * L'_{n_i}(\xi) = 0 \quad , \quad (1 - \eta^2) * L'_{n_i}(\eta) = 0 \quad (18)$$

where,  $L'_{n_i}$  is first derivative of Lagrange polynomials of degree  $n_i$ .

By using these control points, the computational errors decrease exponentially. This method can converge faster to the exact solution than FEM due to using fewer degrees of freedom with almost the same accuracy. Control points make the mass matrix diagonal, which saves time and memory efficiently.

Differential elements of area  $dxdy$  within a given quadrilateral element  $\Omega_e$  is related to differential elements of area  $d\xi d\eta$  in the master square by

$$dxdy = J_e d\xi d\eta \quad (19)$$

Where  $J_e$  denotes the Jacobian of the transformation:

$$J_e = \begin{vmatrix} \frac{\partial x}{\partial \xi} & \frac{\partial y}{\partial \xi} \\ \frac{\partial x}{\partial \eta} & \frac{\partial y}{\partial \eta} \end{vmatrix} \quad (20)$$

On each elements  $\Omega_e$ , a function  $f$  is interpolated by products of Lagrange polynomials of degree  $n_i$  as:

$$f(\bar{x}(\xi, \eta)) \approx \sum_{a=1}^{n_x} N_a(\xi, \eta) f_a = \sum_{p=0}^{n_i} \sum_{q=0}^{n_i} h_p(\xi) h_q(\eta) f_{pq} \quad (21)$$

where the coefficients  $f_{pq}$  are the functional values of  $f$  at the interpolation points  $\bar{x}(\xi_p, \eta_q)$ .

following form:

$$f_{pq} = f(\bar{x}(\xi_p, \eta_q)) \quad (22)$$

In the SFEM, integrations of the matrices may be approximated using the Legendre-Gauss-Lobatto (LGL) quadrature rule in integration over the elements  $\Omega_e$ :

$$\int_{\Omega_e} f(\bar{x}) dxdy = \int_{-1}^1 \int_{-1}^1 f(\bar{x}(\xi, \eta)) J_e(\xi, \eta) d\xi d\eta \approx \sum_{p,q=0}^{n_i} \omega_p \omega_q f_{pq} J_{e(pq)} \quad (23)$$

$w_p, w_q$  are the weights associated with the LGL points of integration, and  $J_{e(pq)} = J_e(\xi_p, \eta_q)$ .

A highly interesting property of the SFEM is the fact that the mass matrix [M] is diagonal due to using LGL quadrature for each element (Komatitsh et al, 1999, [23]). This allows for a very significant reduction in computational cost and complexity.

### 2.3. Time integration of general system

To solve the system of differential equations (Eq. 9), several numerical methods are available. In numerical methods, two factors of stability and accuracy are highly significant. Among the most applicable ones are Newmark Method and Central Difference Method. The Newmark Method, with  $\delta = 0.5$  and  $\alpha = 0.25$ , is unconditionally stable; on the contrary the Central Difference Method is conditionally stable. Selection of time step  $\Delta t$  is another factor which must be taken into account when solving the system of equations. Number of the time steps influences directly the computation volume and the needed accuracy. In SFEM, in high orders, the intervals between the nodes are smaller than those of the FEM. Therefore, smaller time steps are needed for high-order spectral elements. In this study Newmark numerical integration method has been used for solving the system of differential equations.

Like the other types of numerical methods based on meshing, in the SFEM, spatial separation is controlled by the elements' size and the degree of the polynomial order used in interpolation functions in each element  $n_i$ . If the degree of the polynomial order,  $n_i$ , is very low (for example, less than 4), the SFEM brings about inaccuracies, similar to FEM used in problems of wave propagation (Marfurt, 1984) [28]. On the other hand, a high-order polynomial (for example, more than 15) makes this method very accurate, but the computation costs will be increased. In SFEM used for the problems of wave propagation, applying a polynomial with an order ranging from 5 to 10, the best balance will be provided between

accuracy and cost (Seriani and Priolo, 1994) [29].

### 3. Program Verification

A two-dimensional spectral finite element code named as NASEM was developed based on the above mentioned formulation. Two numerical examples are presented in order to demonstrate the accuracy, efficiency and capability of the SFEM in carrying out site response analysis of topographical structures in time domain. All quantities are measured in SI.

#### 3.1. Example 1: site response analysis of a single layer on half-space (1D analysis)

The purpose of this example is to illustrate the applicability and accuracy of the presented SFEM formulation in performing site response analysis of a 1D uniform homogeneous soil layer resting on a rigid bed rock and subjected to vertically propagating incident SV waves. The shear wave velocity of the soil layer was chosen as 300 m/s, its Poisson ratio was 1/3, its damping ratio was 0.05, its mass density was 2.0 t/m<sup>3</sup> and its thickness was chosen as 50 m. The incident wave was chosen as the well known Ricker type (Fig. 2) with the following equation:

$$f(t) = A_{\max} [1 - 2(\pi f_p (t - t_0))^2] e^{-(\pi f_p (t - t_0))^2} \quad (24)$$

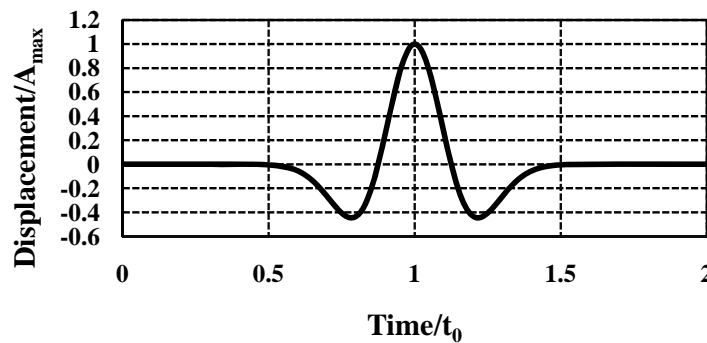


Fig. 2 Displacement time history of the incident wave

where  $f_p$ ,  $t_0$  and  $A_{\max}$  denote the predominant frequency, the time shift parameter and the maximum amplitude of the displacement time history, which were chosen as 2.4 Hz, 0.9 s and 0.0001 m, respectively.

Fig. 3 shows the mesh geometry used for the solution of the problem. The lateral boundaries of the soil layer were placed at a distance of 5000 m from each other (50

times the thickness of the soil layer) i.e. sufficiently far away from its center in order to simulate the 1D condition at the centerline. A number of 1250 spectral finite elements were used in order to discretize the area. In all elements, the ratio of length to width was selected as 2. The numerical analysis was executed using polynomials of degree 4 and a time step of equal to 0.005 s.

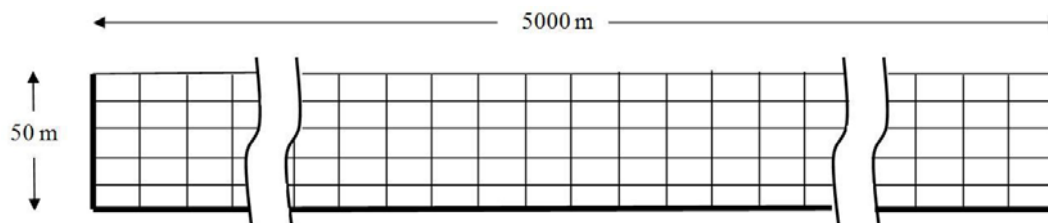


Fig. 3 Geometry and discretization of the 1D single layer on rigid half-space in example (1) by the SFEM

Meanwhile, the same problem was analyzed once again using the well known Plaxis code [30] in order to validate the numerical results obtained by the SFEM. PLAXIS is a conventional isoparametric finite element program developed for geotechnical applications. Quadratic 6-node and 4th order 15-node triangular elements can be used in order to discretize the problem. Either fixed or proper absorbent boundary conditions can be used in order to model the lateral boundary conditions. In 1D site response analysis problems, the input motion will be subjected to the bottom boundary.

In the FEM analysis, two models were analyzed with two different widths of 4000 and 5000 m, respectively. A total number of 3136 and 3524 quadratic triangular finite elements with medium size were used in order to discretize these two models, respectively. Fixed lateral boundary conditions were used; because the distance between the lateral boundaries was long enough in order to prevent the reflected error waves disturb the 1D response of the ground surface at the middle point. The reason of changing the distance between the lateral boundaries from 4000 to 5000 m was to become assured that these boundaries do

not affect the 1D response at the centerline.

Fig. 4 demonstrates the amplification curves obtained by the FEM code [30] at the top of the centerline. The amplification ratio was defined as the ratio of the Fourier spectrum of the acceleration time history at the ground surface to the Fourier spectrum of the acceleration time history at the bed rock. As can be seen, the amplification curves coincide and it is herewith confirmed that the lateral boundaries are sufficient far away from each other and do not affect the 1D site response at the centerline. Figs. 5 and 6 demonstrate the horizontal normalized

acceleration time history as well as the amplification curve obtained by the SFEM and the FEM code at the top of the centerline, respectively. As it can be seen, an excellent agreement exists between the presented results.

Fig. 6 shows that the maximum amplification ratio occurs at a frequency of 1.5 Hz, which matches the well known natural frequency formula ( $f_n=V_s/4H$ ) of a single soil layer (Kramer (1996) [31]), where  $V_s$  and  $H$  denote the shear wave velocity and thickness of the soil layer, respectively.

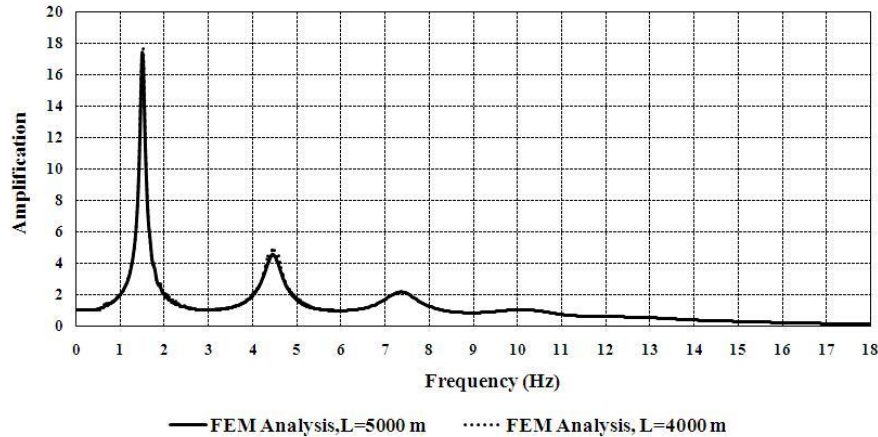


Fig. 4 Comparison of the 1D amplification curves obtained for the single soil layer (at top of the centerline) by the FEM for the two widths of 4000 and 5000 m

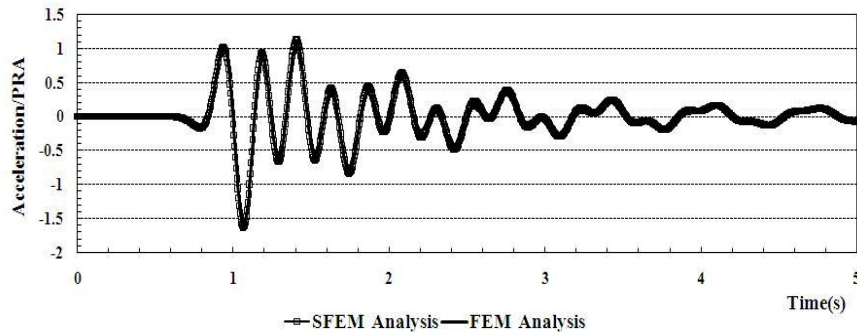


Fig. 5 Normalized (to PRA) acceleration time histories obtained by the SFEM and the FEM at top of the soil layer in the 1D example

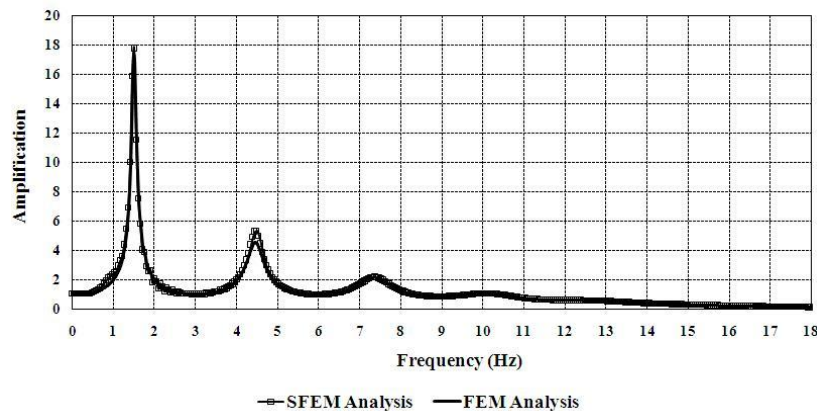


Fig. 6 Comparison of the 1D amplification curves obtained for the single soil layer (at top of the centerline) by the SFEM and the FEM

### 3.2. Example 2: site response analysis of a rectangular alluvial valley (2D analysis)

The purpose of this example was to illustrate the applicability, accuracy and efficiency of the presented SFEM formulation in performing site response analysis of a 2D alluvial valley subjected to vertically propagating incident SV waves. The depth and width of the valley were chosen as 50 and 250 m, respectively. The rock was assumed as rigid. The shear wave velocity of the filling soil, its Poisson ratio, its damping ratio and its mass density were chosen as 400 m/s, 1/3, 0.05 and 2.0 t/m<sup>3</sup>, respectively. The incident wave was chosen again as the well known Ricker type with a predominant frequency of 3 Hz, a time shift parameter of 0.9 s and maximum amplitude of 0.005 m.

Fig. 7 shows the mesh geometry used to solve the problem. A number of 100 spectral finite elements were used in order to discretize the area. In all elements, the ratio of length to width was selected equal to 1. The numerical analysis was executed using polynomials of degree 5 and a time step of 0.01 s. Meanwhile, the same problem was analyzed once again using the Plaxis code [30] in order to validate the numerical results obtained by the SFEM. In the FEM model, a number of 914 quadratic triangular finite elements with medium size were used in order to discretize the area.

Figs. 8 and 9 demonstrate the horizontal normalized acceleration time histories as well as the amplification

curves obtained by the SFEM and the FEM at top of the centerline, respectively. As it can be seen, an excellent agreement exists between the presented results.

Fig. 10 demonstrates the amplification curves obtained by the SFEM at the top of the centerline for four different polynomial degrees ( $N_i = 2, 3, 4$  and 5). As can be seen, if polynomials with a degree of more than 3 are used, excellent accuracies would be obtained. Figures 11 and 12 demonstrate the amplification curves obtained at the same point via different polynomial degrees for the cases that 50 and 20 spectral finite elements, respectively, are used in order to discretize the area. As it can be seen and as expected, decreasing the number of elements requires using polynomials with larger degrees in order to obtain the same excellent accuracies. In the case that 50 spectral elements are used in order to discretize the area, polynomials with a degree of at least 4 are required. In the case that only 20 spectral elements are used in order to discretize the area, polynomials with a degree of at least 5 are required. Table 1 compares the run time needed by the SFEM for the above mentioned combinations of polynomial degrees and mesh sizes. As can be seen and as expected, decreasing the polynomial degree decreases the run time. Using a number of 20 elements with a polynomial degree of 5, a run time of only 18 second is needed in order to analyze the problem and obtain acceptable results by the SFEM which shows it is advantageous over the classic FEM.

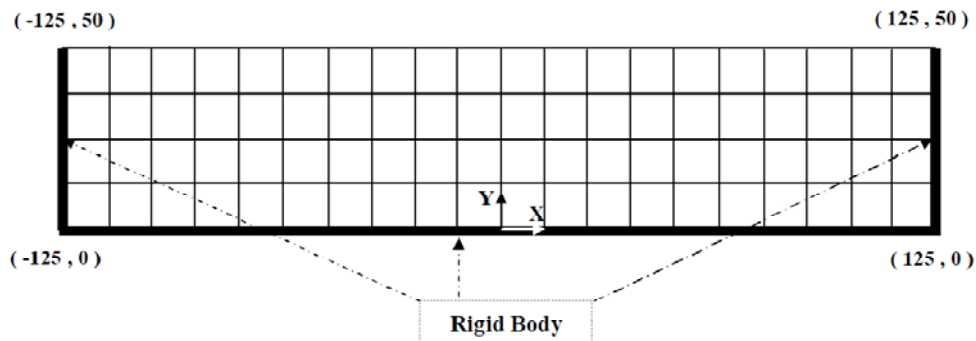


Fig. 7 Geometry and discretization of the 2D rectangular alluvial valley example (2) by the SFEM

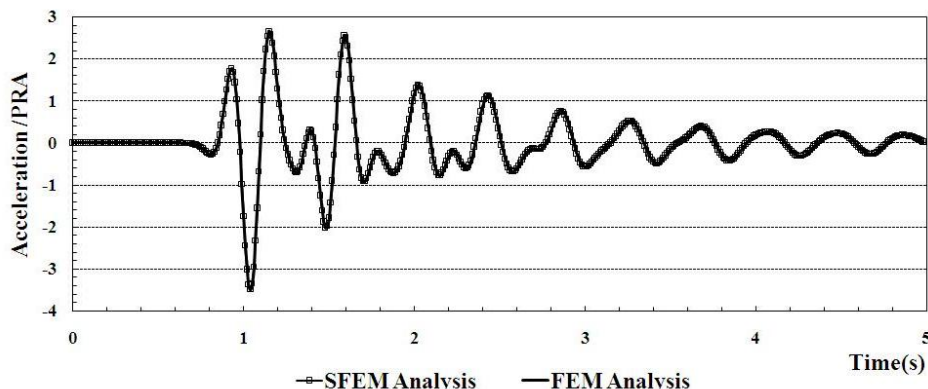
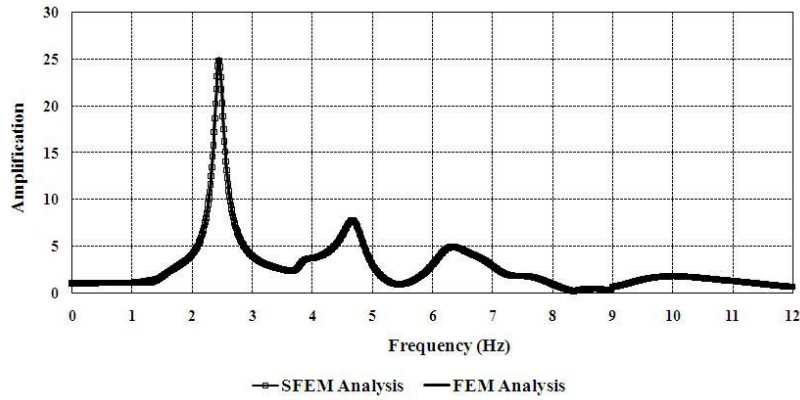
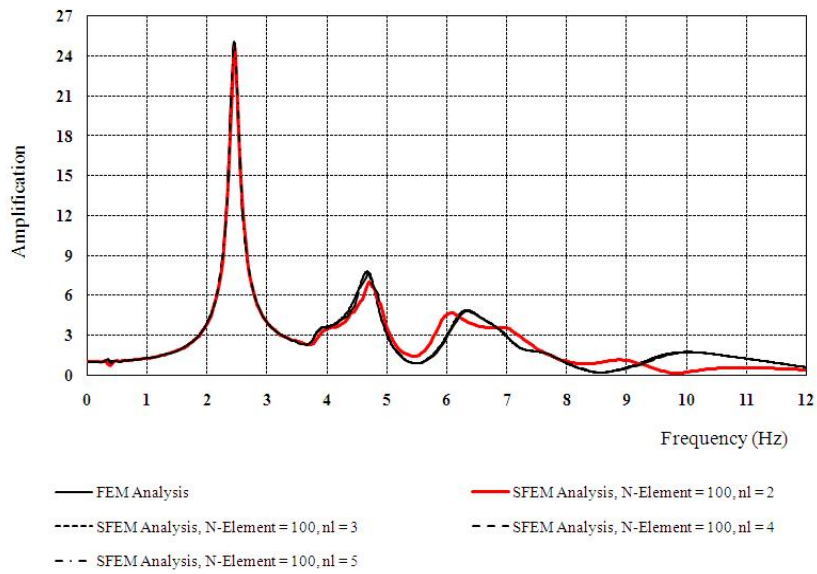


Fig. 8 Comparison of the normalized (to PRA) acceleration time histories obtained by the SFEM and the FEM at the top central point of the rectangular alluvial valley



**Fig. 9** Comparison of the 2D amplification curves obtained by the SFEM and the FEM at top of the center line of the rectangular alluvial valley with a width of 250 m



**Fig. 10** Comparison of the 2D amplification curves obtained by the SFEM at top of the center line of the rectangular alluvial valley for four different polynomial degrees ( $N_1 = 2, 3, 4$  and  $5$ ) and 100 spectral finite elements

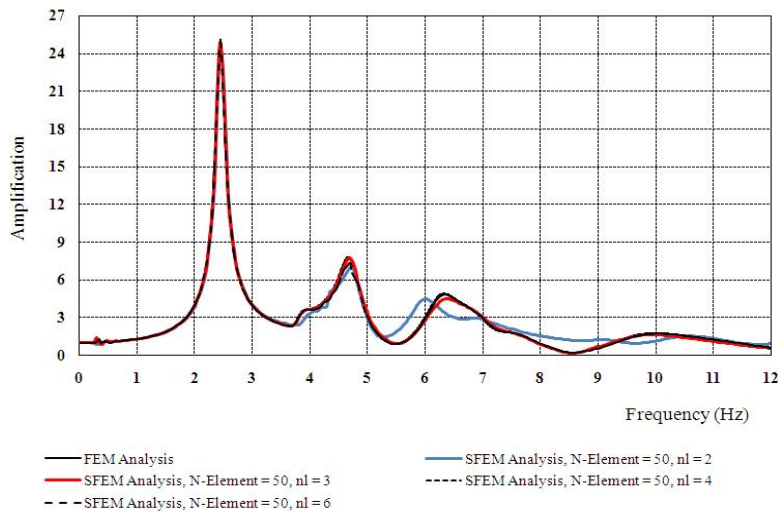


**Fig. 11** Comparison of the amplification curves obtained by the SFEM at top of the centerline of the rectangular alluvial valley for four different polynomial degrees ( $N_1 = 2, 3, 4$  and  $6$ ) and 50 spectral finite elements

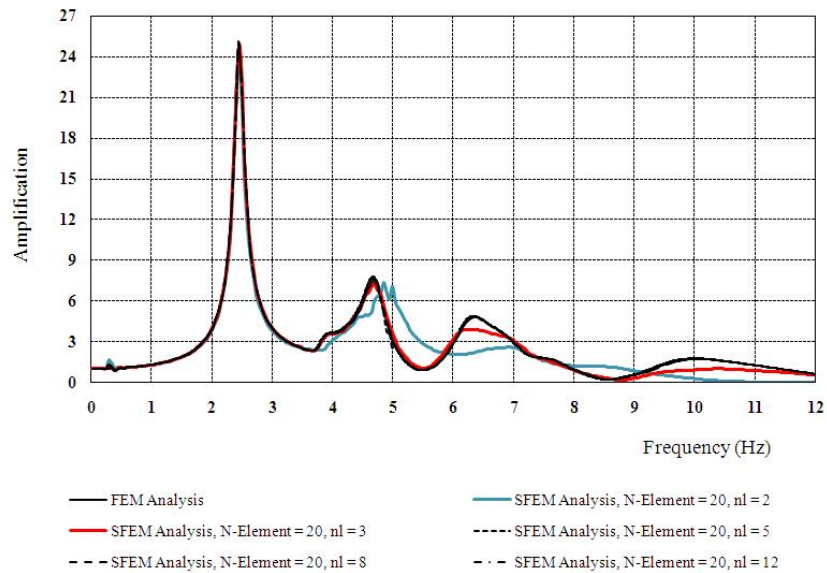


**Fig. 12** Comparison of the amplification curves obtained by the SFEM at top of the centerline of the rectangular alluvial valley for five different polynomial degrees ( $N_1 = 2, 3, 5, 8$  and  $12$ ) and 20 spectral finite elements

**Table 1** Comparison of the run time needed by the SFEM for various combinations of polynomial degree and mesh sizes

Method of Analysis	Number of Element	Polynomials of Degree	Time (s)	Results
SFEM	100	2	1.156	Not Ok
	100	3	28.55	Ok
	100	4	171.03	Ok
	100	5	581.19	Ok
	50	2	0.4	Not Ok
	50	3	5.89	Not Ok
	50	4	40.36	Ok
	50	6	350.23	Ok
	20	2	0.2	Not Ok
	20	3	1.078	Not Ok
	20	5	17.38	Ok
	20	8	216.2	Ok
FEM	914	-	1898	Ok

## 4. Paraemtric Study

### 4.1. Problem posing and model verification

The geometry of the 2-D homogenous rectangular alluvial valley investigated by the parametric study was defined in Fig. 13 where  $H$  and  $ax$  denote the thickness and the half-width of the soil layer, respectively. The thickness of the soil layer was selected as 50 m. Six different shape ratios ( $H/ax$ ) of 0.2, 0.4, 0.6, 0.8, 1.0 and 2.0 encountered frequently in the nature were considered. The shear wave velocity of the soil layer was chosen as 300 m/s, its Poisson ratio was chosen as  $1/3$  and its

damping ratio was 0.05. Only one value of Poisson ratio was considered because previous works [32] showed that the Poisson ratio of the media has a less important effect on the seismic behavior of topographic features in comparison with the shape ratio. As only the amplification curves along the surface of the valley was aimed to be studied, the same vertically propagating incident SV wave of the Ricker type (Fig. 2) was subjected to the valley. Because altering the input motions would not affect the amplification pattern in a linear elastic media. A number of 400 spectral elements, a time step of equal to 0.005s and a polynomial degree of 5 or 36 control points was used in the numerical analysis.

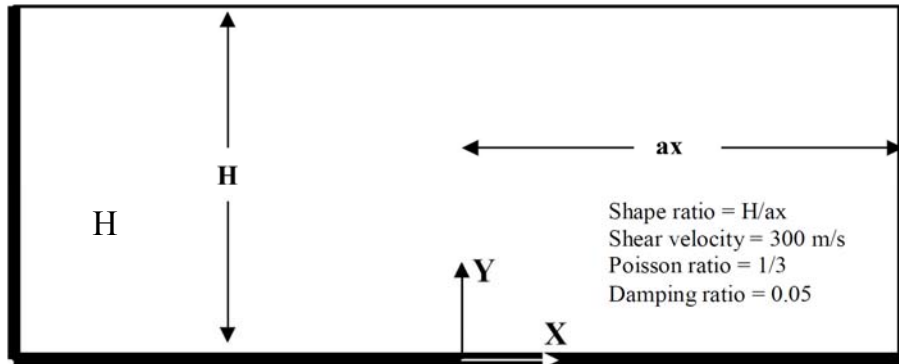


**Fig. 13** Geometry of the 2-D rectangular alluvial valley investigated by the parametric study.  $H$  and  $ax$  denote the thickness and the half-width of the soil layer, respectively

#### 4.2. Results

Fig. 14 demonstrates the amplification curves of various nodes along the ground surface via the different shape ratios. As can be seen, the amplification pattern of the rectangular alluvial valley and its frequency characteristics depend strongly on its shape ratio. In each rectangular alluvial valley and irrespective of its shape ratio, the maximum amplification ratio at each node along the ground surface occurs at a characteristic frequency which is uniform along the ground surface. This characteristic frequency could be named as the natural frequency of the rectangular alluvial valley. The value of

the natural frequency of the rectangular alluvial valley decreases as the shape ratio decreases and tends towards the natural frequency of the corresponding 1D uniform soil layer over the bed rock ( $W = Vs/4H$ ). Vice versa and as expected, the value of the natural frequency of the rectangular alluvial valley increases as its shape ratio increases. This is because reducing the width of the valley means confining a much lesser mass of alluvial by the rigid bed rock which results in increasing the stiffness of the alluvial in the horizontal direction. It can also be seen that in each rectangular alluvial valley and irrespective of its shape ratio, the maximum amplification ratio along the ground surface occurs at the center.

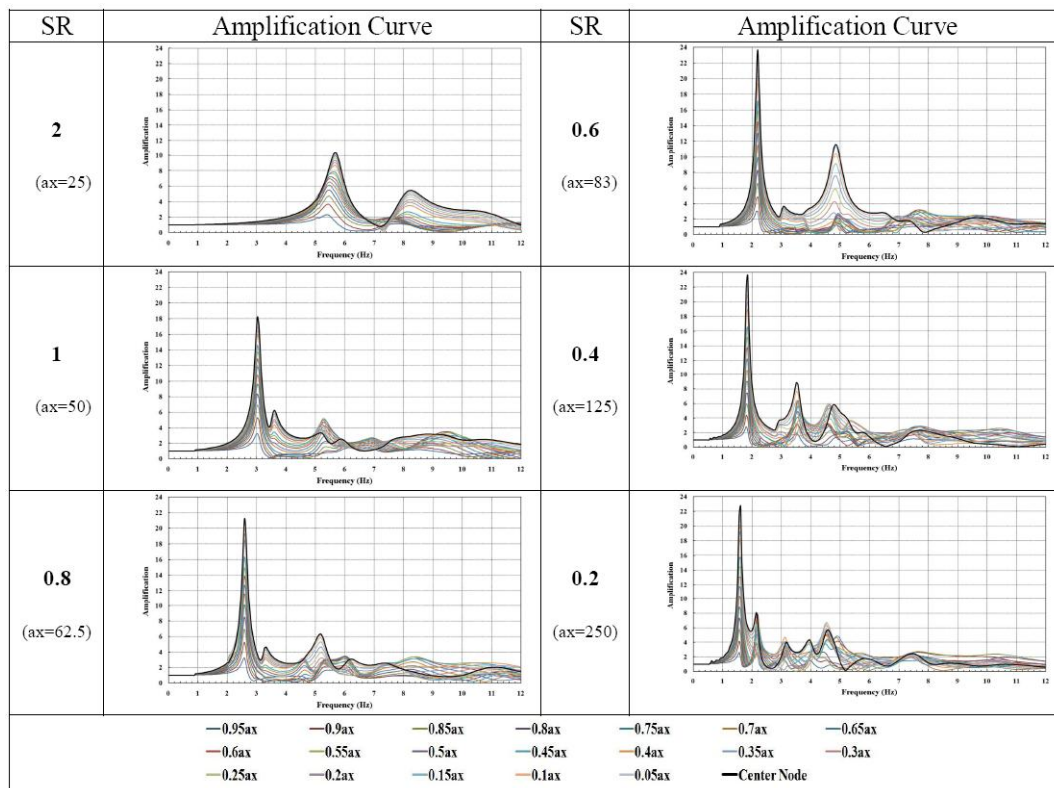


**Fig. 14** Variation of the amplification curves along the ground surface of the rectangular alluvial valley ( $V_s = 300$  m/s) via different shape ratios

Fig. 15 demonstrates how the maximum amplification ratio changes along the rectangular alluvial valley via the different shape ratios. As can be seen, it is once again confirmed that in each rectangular alluvial valley and irrespective of its shape ratio, the maximum amplification ratio along the ground surface occurs at the center of the valley and when one moves from each of the corners towards the center, the maximum amplification ratio of the ground surface increases. No clear relation could be detected between the maximum amplification ratio and the shape ratio of the rectangular alluvial valley. The amplification potential of the rectangular alluvial valley gets its maximum value at a shape ratio of 0.6, decreases gradually as the shape ratio decreases from 0.6 to 0.2 and decreases gradually too, as the shape ratio increases from 0.6 to 2.

Fig. 16 demonstrates the amplification curves of the center of the rectangular alluvial valley with different shape ratios and compares them with the amplification curve of the corresponding 1D uniform soil layer over the bed rock. As can be seen, when the shape ratio decreases, the natural frequency of the rectangular alluvial valley decreases and the amplification curve of the center node (2D case) moves towards the amplification curve of the corresponding 1D case. Although in all rectangular alluvial valleys with shape ratio of less than one, the maximum amplification ratio at the center node is more than that corresponding to the 1D case, but in the

rectangular alluvial valley with a shape ratio of 2 the converse case was detected.

Extracting a simple formula in order to get an initial estimation of the natural period of a rectangular alluvial valley could be useful in site effect microzonation studies. Fig. 17 demonstrates how the natural frequency of the rectangular alluvial valley alters with its shape ratio. Two curves are presented that corresponds to two different alluvials with a shear wave velocity of 300 and 400m/s, respectively. As can be seen, the curves are similar and infuse the idea of being capable to become non-dimensionalized. Fig. 18 demonstrates these two curves once again, this time normalized to the natural frequency of the corresponding 1D uniform soil layer over the bed rock. As expected, the curves coincide and the ratio of the natural frequency of a rectangular alluvial valley ( $F_{2D}$ ) to the natural frequency of the corresponding 1D uniform soil layer over the bed rock ( $F_{1D}$ ) can be approximated as a function of the shape ratio by the following formula:

$$F_{2D}/F_{1D} = 0.958 \cdot \exp(0.699 \cdot SR)$$

which can be re-written as:

$$F_{2D} = 0.958 \cdot \exp(0.699 \cdot SR) \cdot (V_s / (4 \cdot H))$$

Where,  $V_s$  represents shear wave velocity,  $H$  rectangular valley depth, and  $SR$  the valley shape ratio ( $SR=H/ax$ ).

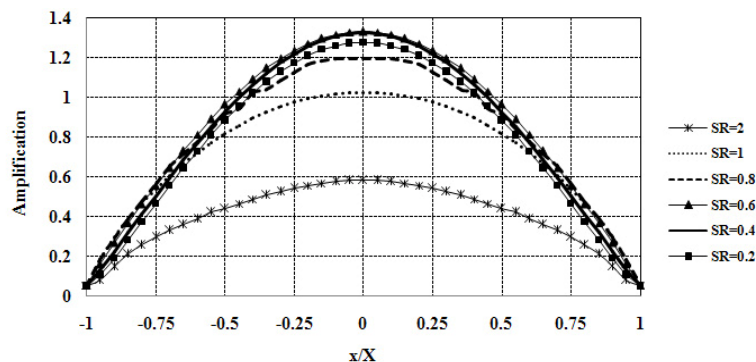


Fig. 15 Variation of the maximum amplification ratio along the ground surface of the rectangular alluvial valley ( $V_s = 300$  m/s) via different shape ratios

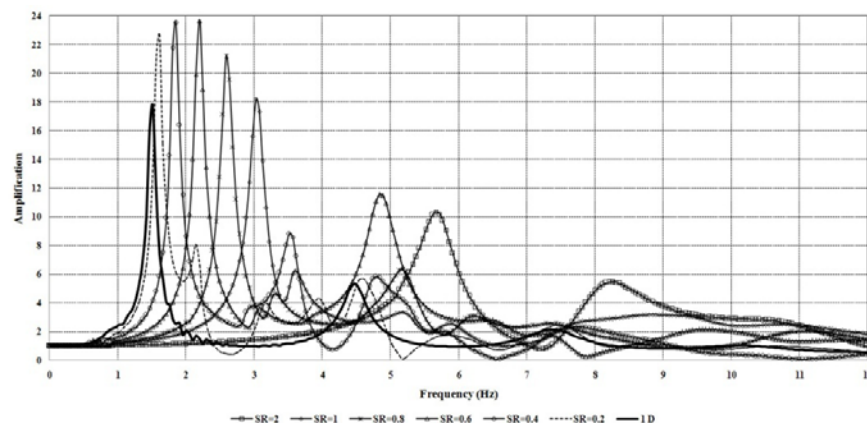


Fig. 16 Amplification curves at top of the centerline of the rectangular alluvial valley ( $V_s = 300$  m/s) with different shape ratios

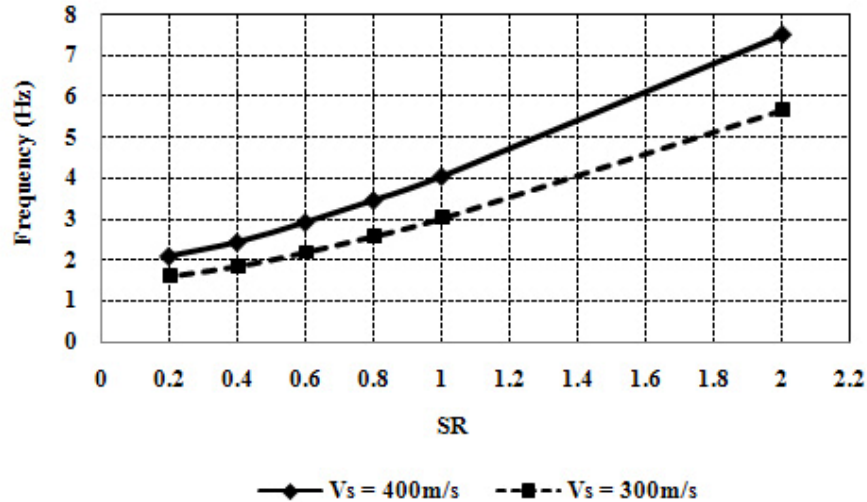


Fig. 17 Natural frequency of the rectangular alluvial valley via its shape ratio for two different shear wave velocities of 300 and 400 m/s

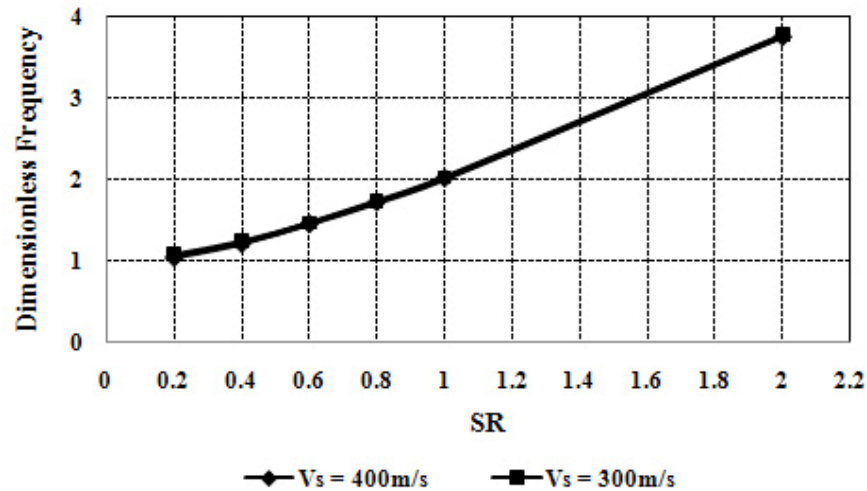


Fig. 18 Dimensionless frequency of the rectangular alluvial valley via its shape ratio

### 5. Conclusion

In this paper, an advanced formulation of 2D SFEM in time-domain is presented and implemented in order to carry out site response analysis of topographic structures subjected to vertically propagating in-plane incident shear waves. The accuracy, efficiency and applicability of the formulation are demonstrated through some numerical examples of 1D and 2D site response analysis problems. A numerical parametric study was carried out on the seismic response of rectangular alluvial valleys subjected to vertically propagating incident SV waves. It is shown that the amplification pattern of the rectangular alluvial valley and its frequency characteristics depend strongly on its shape ratio. A natural frequency can be defined for the rectangular alluvial valley so that at all nodes along the ground surface, the highest amplification factor occurs at

this predominant frequency. The natural frequency of the rectangular alluvial valley decreases towards the natural frequency of the corresponding 1D uniform soil layer on bed rock, as the shape ratio of the valley decreases. The maximum amplification ratio along the ground surface occurs at the center of the valley and decreases when one moves towards the corners. A simple formula has been proposed for initial estimation of the natural period of rectangular alluvial valleys which can be used in site effect microzonation studies.

### References

- [1] Bouchon M. Effect of Topography on Surface Motion, Bulletin of the Seismological Society of America, 1973, Vol. 63, pp. 615-632.
- [2] Zhang C, Zhao C. Effects of canyon topography and geological conditions on strong ground motion, Earthquake Engineering & Structural Dynamics, 1988,

- Vol. 16, pp. 81-97.
- [3] Zhao C, Valliappan S. Incident P and SV wave scattering effects under different canyon topographic and geological conditions, *International Journal for Numerical and Analytical Methods in Geomechanics*, 1993, No. 2, Vol. 17, pp. 73-94.
- [4] Sincaian MV, Oliveira CS. Nonlinear seismic response of a volcanic hill using the Finite element method, *Soil Dynamics and Earthquake Engineering*, 2000, Vol. 20, pp. 145-154.
- [5] Geli L, Bard PV, Julien B. The Effect of Topography on Earthquake Ground Motion: A Review and New Results, *Bulletin of the Seismological Society of America*, 1988, Vol. 78, pp. 42-63.
- [6] Kamalian M. Time Domain Two-Dimensional Hybrid FEM / BEM Dynamic Analysis of Non-Linear Saturated Porous Media, Ph.D. Dissertation, Tehran University, 2001 [In Persian].
- [7] Kamalian M, Jafari MK, Dehghan K, Sohrabi-Bidar A, Razmkhah A. Two-Dimensional Hybrid Response Analysis Of Trapezoidal Shaped Hills In Time Domain, *Advances in Boundary Element Techniques IV*, Ed. R. Gallego, MH. Aliabadi, 2003, pp. 231-236.
- [8] Kamalian M, Gatzmiri B, Sohrabi A. On time-domain two-dimensional site response analysis of topographic structures by BEM, *Journal of Seismology and Earthquake Engineering*, 2003, No. 2, Vol. 5, pp. 35-45.
- [9] Kamalian M, Jafari MK, Sohrabi-bidar A. Transient site response analysis of nonhomogenous two-dimensional topographic features by BEM, *Esteghlal Journal of Engineering*, 2006, No. 2, Vol. 24, pp. 51-68, [In Persian].
- [10] Kamalian M, Jafari MK, Sohrabi-Bidar A, Razmkhah A, Gatzmiri B. Time-domain two-dimensional site response analysis of non-homogeneous topographic structures by a hybrid FE / BE method, *Soil Dynamics and Earthquake Engineering*, Vol. 26, pp. 753-765.
- [11] Kamalian M, Jafari MK, Sohrabi-bidar A, Razmkhah A. Numerical Seismic Behavior Assesment of the 2D Hills Subjected To Vertically Propagating Incident P and SV Waves, Research Project, IIEES Report, Tehran, Iran, 2005 [In Persian].
- [12] Kamalian M, Jafari MK, Sohrabi-bidar A. Seismic behaviour of 2D semi-sine shaped hills against vertically propagating incident waves, *Esteghlal, Journal of Engineering*, No. 1, Vol. 26, pp. 109-130 [In Persian].
- [13] Kamalian M, Jafari MK, Sohrabi-bidar A, Razmkhah A. Amplification pattern of 2D trapezoidal shaped hills subjected to vrtically propagating incident waves, *Modares, Technical and Engineering Journal*, 2007, Vol. 29, pp. 11-30 [In Persian].
- [14] Kamalian M, Jafari MK, Sohrabi-bidar A, Razmkhah A. Shape effects on amplification potential of two-dimensional hills, *Journal of seismology and earthquake engineering*, 2006, No. 2, Vol. 8, pp. 59-70 [In Persian].
- [15] Sohrabi-Bidar A. Seismic Behavior Assessment of Surface Topographies Using Time Domain 3D Boundary Elements Method, Ph.D. Dissertation, International Institute of Earthquake Engineering and Seismology, 2008 [In Persian].
- [16] Sohrabi-Bidar A, Kamalian M, Jafari MK. Time-domain BEM for three-dimensional site response analysis of topogaphic structures, *International Journal for Numerical Methods in Engineering*, 2009, No.79, PP.1467-1492.
- [17] Chaljub E, Komatitsch D, Vilotte J, Capdeville Y, Valette B, Festa G. Spectral-Element Analysis in Seismology, France: IASPEI, 2005.
- [18] Khaji N, Habibi M, Mirhashemian P. Modeling transient elastodynamic problems using spectral element method, *Asian Journal of Civil Engineering (Building and Housing)*, 2009, No. 4, Vol. 10, pp. 361-380.
- [19] Patera AT. A Spectral element method for fluid dynamics: laminar flow in a channel expansion, *Journal of Computational Physics*, Vol. 54, pp. 468-488.
- [20] Cohen G, Joly P, Tordjman N. Construction and analysis of higher-order finite elements with mass lumping for the wave equation, *Proceedings of the Second International Conference on Mathematical and Numerical Aspects of Wave Equation*, edited by R. Kleinman, SIAM, Philadelphia, PA, 1993, pp. 152-160.
- [21] Komatitsch D. M'ethodes spectrales et 'el'ements spectraux pour l'equation de l'elastodynamique 2D et 3D en milieu h'et'erog'ene (Spectral and spectral-element methods for the 2D and 3D elastodynamics equations in heterogeneous media, Ph.D. thesis, Institut de Physique du Globe, Paris, France, in French, 1997, 187 p.
- [22] Komatitsch D, Vilotte JP. The spectral-element method: an efficient tool to simulate the seismic response of 2D and 3D geological structures, *Bulletin of the Seismological Society of America*, 1998, No. 2, Vol. 88, pp. 368-392.
- [23] Komatitsch D, Tromp J. Introduction to the spectral element method for three-dimensional seismic wave propagation, *Geophysical Journal International*, 1999, Vol. 139, pp. 806-822.
- [24] Komatitsch D, Barnes Ch, Tromp J. Simulation of anisotropic wave propagation based upon a spectral element method. *Geophysics*, No. 4, July-Agust, Vols. 65, pp. 1251-1260.
- [25] Komatitsch D, Tromp J. Spectral-element simulations of global seismic wave propagation-II.3-D models, oceans, rotation, and self-graviation, *Geophysical Journal International*, Vol. 150, pp. 303-318.
- [26] Komatitsch D, Tsuboi S, Tromp J. The spectral-element method in seismology, *Seismic Earth*, 2005, Vol. 157, pp. 205-227.
- [27] Komatitsch D, Vilotte JP, Vai R, Castillo-Covarrubias JM, Sanchez-Sesma FJ. The spectral element method for elastic wave equations-application to 2-D and 3-D seismic problems, *International Journal for Numerical Methods in Engineering*, 1999, Vol. 45, pp. 1139-1164.
- [28] Marfurt KJ. Accuracy of finite-difference and finite-element modeling of the scalar wave equation, *Geophysics*, 1984, Vol. 49, pp. 533-549.
- [29] Seriani G, Priolo E. Spectral element method for acoustic wave simulation in heterogeneous media, *Finite Elements in Analysis and Design*, 1994, Vol. 16, pp. 337-348.
- [30] PLAXIS, Finite Element Code, Copyright 1997-2008 Plaxis BV, 2008.
- [31] Steven K. Kramer. *Geotechnical Earthquake Engineering*, Prentice- Hall, Inc, 1996.
- [32] Kamalian M, Jafari MK, Sohrabi Bidar A, Razmkhah A. Seismic response of 2D semi-sine shaped hills to vertically propagating incident waves: amplification patterns and engineering applications, *Earthquake Spectra (ISI)*, 2008, No. 2, Vol. 24, pp. 405-430.